Membranes

DOI: 10.1002/ange.201408417

Mapping Conformational Heterogeneity of Mitochondrial Nucleotide Transporter in Uninhibited States**

*Remy Sounier, Gaetan Bellot, and James J. Chou**

Abstract: *One of the less well understood aspects of membrane transporters is the dynamic coupling between conformational change and substrate transport. NMR approaches are used herein to investigate conformational heterogeneity of the GTP/GDP carrier (GGC) from yeast mitochondria. NMR residual dipolar coupling (RDC) analysis of GGC in a DNA-origami nanotube liquid crystal shows that several structured segments have different generalized degrees of order (GDO), thus indicating the presence of conformational heterogeneity. Complete GDO mapping reveals asymmetry between domains of the transporter and even within certain transmembrane helices. Nucleotide binding partially reduces local structural heterogeneity, and the substrate binds to multiple sites along the transport cavity. These observations suggest that mitochondrial carriers in the uninhibited states are intrinsically plastic and structural plasticity is asymmetrically distributed among the three homologous domains.*

Most solute transporters in membranes adopt the so-called alternating access mode of transport, in which access to the central binding site by the substrate can switch between opposite sides of the membrane.[1] This mechanism involves at least two conformational states: the outward-facing open conformation where the substrates can enter the binding site from the extracellular space and the inward-facing conformation where the binding site is exposed to the intracellular compartment, for the release of the bound substrate and for receiving new substrates.[1,2]

A recurring theme in these transporters is the presence of conformationally homologous domains, which are related to each other by a distinct symmetry axis. Most of the transporter architectures have a twofold pseudosymmetry[3] with the symmetry axis being parallel to the substrate translocation pathway. These transporters are generally known to switch between the "V" and inverted "V" types of structures during their transport cycles.[4] There are, however, also transporters which adopt threefold pseudosymmetry and their mechanism of transport is less well understood.

A major transporter family with threefold pseudosymmetry is the mitochondrial carrier family. This family of transporters selectively catalyze the trafficking of metabolites, nucleotides, ions, and vitamins across the mitochondrial inner membrane.[2a,5] They are driven mainly by substrate concentration gradient and have been proposed to adopt the alternating access mechanism.[2a,6] To date, structures of only two mitochondrial carriers are available and they all have been determined under inhibited conditions. The structures are from the crystal structures of ADP/ATP carrier (AAC) in complex with carboxyatractyloside (CATR)[7] and the NMR-derived backbone structure of the uncoupling protein 2 (UCP2) in the presence of guanosine diphosphate (GDP).[8] The overall architecture of the carrier protein resembles an open-top container formed with three structurally similar domains, and each domain consists of two packed transmembrane (TM) helices (labelled H) separated in sequence by an amphipathic (AP) helix (labelled *h*; see Figure S1a in the Supporting Information).[7a] The domains contain several conserved sequence/structure motifs, among which the important ones are the proline kinks (P-kinks) of H1, H3, and H5, which act as the "pivots" for the transporter,[2a] and the glycine linker (G-linker) which modulates the relative orientation between TM and AP helices in each domain (Figure S1b).[9] The P-kinks are approximately at the midpoint of the transporter along the membrane normal and divide the transporter into two sections, referred to as the cytosolic section (*c-section*) and matrix section (*m-section*) in this paper (Figure S1a).

NMR spectroscopy is emerging as a technology for investigating conformational dynamics of transporters and ion channels and 7-TM helices receptors, as exemplified by the studies on EmrE,[4b] KcsA,[10] rhodopsin,[11] and β2A receptor.[12] In earlier work, we demonstrated the use of NMR spectroscopy in achieving full-scale characterization of the backbone conformation of a 34 kDa mitochondrial transporter known as UCP2 in the inhibited state.[8] Encouraged by this NMR study, we sought to use NMR techniques to investigate the conformational dynamics of carrier proteins in the uninhibited form to facilitate the understanding of whether the conversion involves purely rigid body movements of the pseudosymmetric protein domains, or whether it also requires intrinsic structural variability on both global and local levels.

[*] Dr. R. Sounier,[+] Dr. J. J. Chou
Department of Biological Chemistry and Molecular Pharmacology
Harvard Medical School, Boston, MA 02115 (USA)
E-mail: chou@crystal.harvard.edu
Dr. G. Bellot
Institut de Génomique Fonctionnelle, Centre National de la Recherche Scientifique (CNRS) Unité Mixte de Recherche (UMR) 5203, Institut National de la Santé et de la Recherche Médicale (INSERM) U1191, Université de Montpellier, F-34000 Montpellier (France)
[+] Present address: Institut de Génomique Fonctionnelle, Centre National de la Recherche Scientifique (CNRS) Unité Mixte de Recherche (UMR) 5203, Institut National de la Santé et de la Recherche Médicale (INSERM) U1191, Université de Montpellier F-34000 Montpellier (France)

[**] This work was supported by the NIH grant GM094608 (to J.J.C.).
Supporting information for this article is available on the WWW under http://dx.doi.org/10.1002/anie.201408417.

The carrier protein we chose for the current study is the GTP/GDP carrier (GGC) from yeast mitochondria.[13] GGC is a 300 amino acid residue transporter which transports external guanosine triphosphate (GTP) into the mitochondrial matrix while exporting internal GDP out of the matrix.[13] The structure of GGC is unknown. Here, we combine dipolar coupling tensor analysis and chemical shift perturbation to investigate the local and global conformational variability of GGC in the absence of substrate and how ligand bindings alter the conformational heterogeneity of GGC.

GGC with a C-terminal His-tag was expressed in E. coli cells, purified, and solubilized in dodecylphosphocholine (DPC) detergent as described in the Supporting Information. The ^{1}H-^{15}N transverse relaxation-optimized spectroscopy (TROSY) spectrum of the reconstituted GGC shows good spectral resolution and resonance intensity (Figure 1). Backbone assignments have been obtained for 94% of all non-proline residues (see Figure S2 and Table S1 in the Supporting Information). We built a structural model of GGC (see Figure S3 in the Supporting Information) based on alignment of signature sequence motifs and secondary structures between GGC and AAC (PDB code: 1OKC). The secondary structures of GGC were determined using a combination of RDC-based (RDC = residual dipolar coupling) molecular fragment replacement (MFR) method[8,14] and NMR chemical shifts (TALOS+)[15] (see Figures S2, S4 and Methods in the Supporting Information).

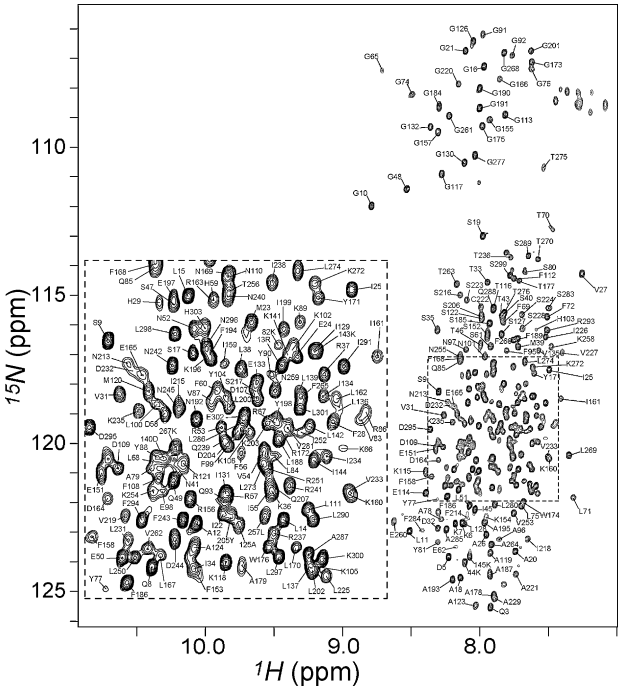

Figure 1. Backbone amide resonance assignments of GGC. The two-dimensional [^{15}N-^{1}H] TROSY-HSQC spectrum of *U*-[^{2}H, ^{15}N, ^{13}C]-GGC in DPC micelles shown here was collected on a Bruker 600 MHz spectrometer with a cryogenic probe at 30°C. Sequence-specific resonance assignments are indicated by the residue labels. To resolve the peaks in the crowded region, the spectrum was over-processed with a sharp apodization function in the ^{1}H dimension with a 63°-shifted squared sine-bell window.

We then used NMR chemical shift perturbation to examine GGC binding with nucleotides including GDP, GTP, and adenosine monophosphate (AMP). We measured NMR resonance shifts using the three-dimensional TROSY HNCO spectrum, which correlates the chemical shifts of backbone ^{1}H, ^{15}N, and $^{13}C'$ nuclides. GDP and GTP both induced substantial chemical shift, whereas the effect of nucleoside monophosphate AMP is insignificant (see Figure S5 in the Supporting Information). This result is consistent with previous observations that GGC in liposomes catalyzed the transport of GTP and GDP with high efficiency, as well as the transport of the corresponding deoxynucleotides and the structurally related inosine di- and triphosphate.[13]

Addition of GDP and GTP to GGC induced similar patterns of chemical shift perturbation (see Figure S6 in the Supporting Information), thus indicating that the two nucleotides have common binding sites and/or same allosteric effect on the carrier. Despite the threefold pseudosymmetric conformation, the chemical perturbation is highly asymmetric. The *m-section* of the protein shows greater substrate-induced chemical perturbation than the *c-section* (see Figure S6e,f). More specifically, the helical segments of the P-kinks and G-linkers in the *m-section* show pronounced chemical shift changes. Among the three similar domains, the N-terminus and C-terminus, H2 of domain I, and *h*2 of domain II show distinctly larger chemical shift perturbation than the rest. The asymmetric and widespread changes in chemical environment induced by nucleotide binding suggest a rather global change in conformation and/or dynamics in GGC upon substrate binding.

To examine substrate affinity, we calculated a residue-specific dissociation constant (K_D) for GDP and GTP (examples of binding saturation curves are shown in Figure 2a; see Figures S7 and S8a in the Supporting Information). The different K_D value observed for different amino acids of the protein suggest multiple binding sites along the transport path (see Table S2 in the Supporting Information). Mapping the K_D values onto the GGC model shows that regions with highest affinity (or lowest K_D) are clustered around the pivot regions above the P-kinks consisting of residues in H1 (24–28), H3 (132, 133), and H5 (228), and the middle regions of H2 (86–90), H4 (176–182), and H6 (276, 281–282; Figure 2b,c and Figure S8b,c). These regions appear to constitute a well-defined, polar binding site for nucleotides at the center of the transporter, and this is consistent with a binding mode proposed earlier based on sequence alignment and the pseudo-threefold symmetry of the mitochondrial carrier family.[9,16,17] Overall, the affinity for GTP [mean K_D value of the central binding site (CBS) = 6.6 mM] is about fourfold stronger than that of GDP (mean K_D value of the CBS = 23 mM). The three- to fourfold difference in substrate affinities is qualitatively consistent with earlier measurements of GGC transport activity wherein the apparent K_M value of GTP and GDP transport are (1.2 ± 0.1) μM and (4.5 ± 0.7) μM, respectively.[13]

In addition to the central binding site, the K_D mapping also revealed two other regions of substrate affinity. One in the *c-section* consisting of the N-terminus of H1 and the C-

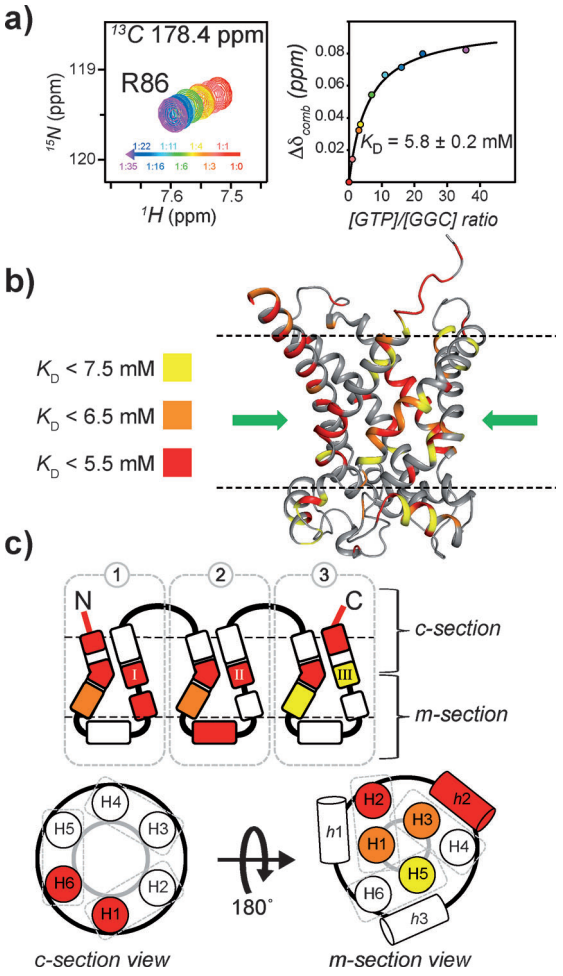

Figure 2. Residue-specific K_D values of GGC-GTP binding. a) Sample chemical shift perturbation from three-dimensional TROSY HNCO spectra of GGC upon incremental addition of GTP. The NMR peaks at different substrate/protein molar ratios are shown with the linear color spectrum scale from ratio = 0 (red) to ratio = 35 for GTP (magenta). For each of the perturbed resonances, the chemical shift changes (defined in the Supporting Information) versus GTP/GGC molar ratio are plotted and fitted to the standard equation of binding equilibrium (right panels). b) Mapping residue-specific K_D values onto the GGC model for GTP binding with color code as defined in the figure. The common binding site (CBS) of nucleotide carrier proteins as proposed based on conservation of amino acids, comparative model, and chemical properties,[16] is indicated by the green arrow. c) The K_D values in (b) are shown in the context of the schematic diagram of the tripartite topology and of the cytoplasmic and matrix views for providing a conceptual view of nucleotide binding sites.

terminus of H6, which may function to initially recruit the substrates to the transporter through charge–charge interactions (Figure 2c). Another region is in the *m-section* and comprises the G-linker of domain I and the amphipathic helix, *h*2 of domain II. It is interesting to note that this region shows not only large chemical shift perturbation (Figure S6c), but also low K_D values (Figure 2c and Figure S8c), thus suggesting that these parts of the GGC play important roles in the binding and transport of nucleotides.

During RDC-based structural analysis of GGC, we found that differently structured segments, as identified by RDC-based MFR, are subject to different alignment tensors, thus indicating that these segments do not align together as a rigid body in solution and that they move or reorient relative to each other. This observation presents a fundamental problem for structure determination: there is not a convergent conformation in the statistical ensemble to be determined, and is in contrast to the previous structure determination of UCP2,[8] a determination which allowed us to refine the entire structure against RDCs without introducing very high dipolar coupling energy. However, RDC can also provide dynamics information complementary to R_1 and R_2 as it covers motions faster than the timescale at which chemical shifts are measured, including the nanosecond and micro- to millisecond motions. We thus used a previously introduced parameter of alignment tensor, known as the generalized degree of order (GDO, ϑ),[18] to investigate local and global conformational heterogeneity. The parameter ϑ_i was determined for all seven-residue segments centered at i along the GGC sequence, except for those that did not have structurally convergent fragments (see Figures S9 and S10 and the in the Supporting Information).

Mapping ϑ_i onto the GGC topology showed that in the absence of substrate, GGC has large global conformational heterogeneity, as the GDO values from the *c*- and *m-sections* of the protein are very different. Moreover, even within the *m-section* of the protein, the GDO values differ significantly between the amphipathic helices (*h*1 and *h*3; Figure 3a) and between the helical segments next to the P-kinks. GTP binding overall reduces GDO dispersion (Figure 3b and Figure 4b) though asymmetric differences persisted between domains, for example, domain I (large perturbation in H2) and domain III (Figure 4b). In contrast, the GDO analysis of the structured fragments of UCP2 bound to the inhibitor GDP shows much less GDO variation (see Figure S11 in the Supporting Information), thus indicating that the conformation of the inhibited UCP2 is more homogeneous. The large differences between the GDO maps of uninhibited GGC and inhibited UCP2 are consistent with the common notion that transporters are generally dynamic and structural homogeneity often requires their inactivation. The analysis of GGC and UCP2 data are also validation of the approach of using GDO as a probe for structural heterogeneity.

To reveal potential local conformational heterogeneity within the secondary elements of GGC, we mapped $\Delta\vartheta_i = |\vartheta_i - \vartheta_{i+3}|$, which is the GDO differences between seven-residue segments that are shifted relative to each other by three residues, onto the GGC topology (Figure 5). In the substrate-free state, H1 and *h*1 of domain I show high local conformational heterogeneity. Although GDO values are not available for the H2 helix of domain I because of missing NMR resonances or lack of convergent fragments, it is likely that this TM helix also undergoes large conformational exchange, which could have broadened the NMR resonances. In addition, the regions of H4 and H5 in the *m-section* show large $\Delta\vartheta_i$. Overall, the *m-section* of the transporter has higher local conformational plasticity than the *c-section*. GTP binding significantly reduces the majority of the $\Delta\vartheta_i$ values, with most pronounced effects localized to the P-kinks and the helical segments following the P-kinks in the *m-section*. This

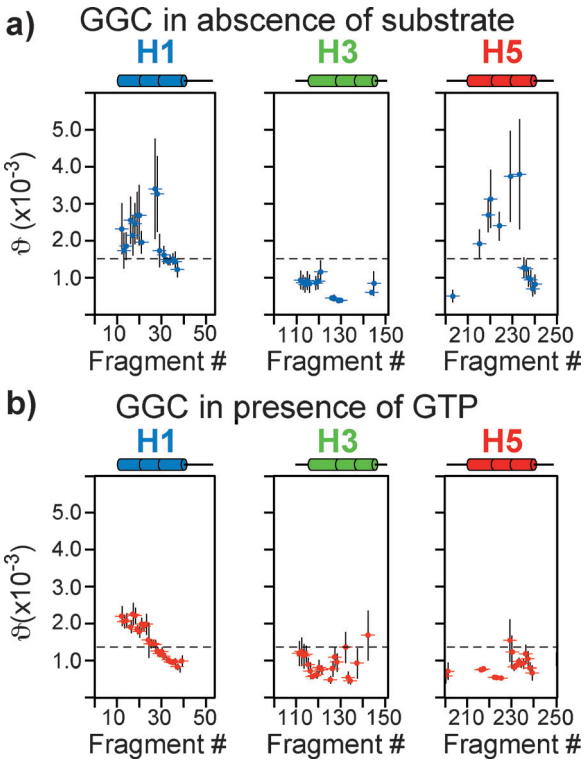

Figure 3. Mapping conformational heterogeneity of the odd helices. GDO variation in GGC in the absence of GTP (a) and in presence of 30 mM of GTP (b), as shown by the plot of GDO values versus the sliding seven-residue fragments for H1, H3, and H5.

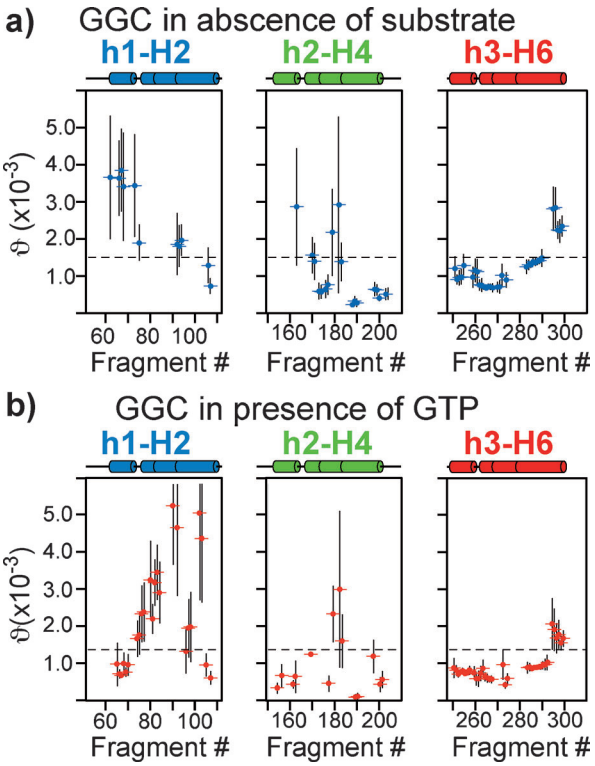

Figure 4. Mapping conformational heterogeneity of the amphipathic and even helices. GDO variation in GGC in the absence of GTP (a) and in the presence of 30 mM of GTP (b), as shown by the plot of GDO values versus sliding seven-residue fragments for H2, H4 and H6.

result suggests that GTP binding partially stabilizes the pivot region of the transporter. But local conformational heterogeneity persists for H2 and *h*1 of domain I and the G-linker of domain II. Similar to the chemical shift perturbation caused by substrate binding, the overall distribution of local and global conformational heterogeneity as indicated by RDC tensor analysis is also highly asymmetric.

The model in Figure 2b, based on the crystal structure of AAC locked in the *c*-state by the inhibitor CATR, confirms the central binding site and shows that it is readily accessible by substrate from the *c*-side, and should thus represent the *c*-state conformation. In addition to the central pivot region, large perturbation in the N-terminus and C-terminus at the *c*-side mouth of the GGC cavity suggests the existence of a secondary binding site in the *c-section* of the protein and may actively recruit substrates before they enter the cavity. Moreover, a large chemical shift perturbation is observed on H2 (see Figure S6e,f). This perturbation can be related to the translocation of the substrate inside the cavity and is consistent with the mechanism of electrostatic funneling of substrate proposed earlier for AAC.[19]

Substrate binding also causes substantial chemical shift change in the *m-section* of all three domains (see Figure S6e,f). In particular, the G-linkers of domain I and the AP helix *h*2 show lower than average K_D values (Figure 2c and Figure S8c). These perturbed residues do not appear to constitute a continuous binding region in our structural model of GGC, which was built based on the *c*-state of AAC. A plausible explanation is that the NMR spectroscopy presents the time and ensemble average of the *c*- and *m*-states. Likewise these observed chemical shift perturbations are due to substrate binding to the *m*-state, which presumably differ significantly from the *c*-state. It is also possible that substrate binding induces conformation change in the *m-section* of the protein, and is also expected to give rise to large chemical shift perturbation. Finally, even in the *c*-state conformation, GGC can conceivably recruit substrate using the highly basic amphipathic helices, for example, an ATP binding site between *h*1 and the loop before *h*2 on the *m*-side of AAC has been proposed based on MD simulation.[20]

GGC in the absence of substrate has large global conformational heterogeneity as indicated by the different GDO values throughout the three domains of the protein. The helical segments in the *c*- and *m-sections* of the transporter also have very different GDO values. These results are consistent with conformational equilibrium between the *c*- and *m*-states of GGC in the absence of ligand. GGC is capable of performing bidirectional transport, that is, GGC reconstituted in liposome can catalyze GDP/GDP and GTP/GTP homoexchange,[13] and the intrinsic "molecular breathing" would allow the entrance of substrates into the transporter from either side of the membrane.

An unexpected finding, however, is that GGC in the absence of substrates also shows large local conformational

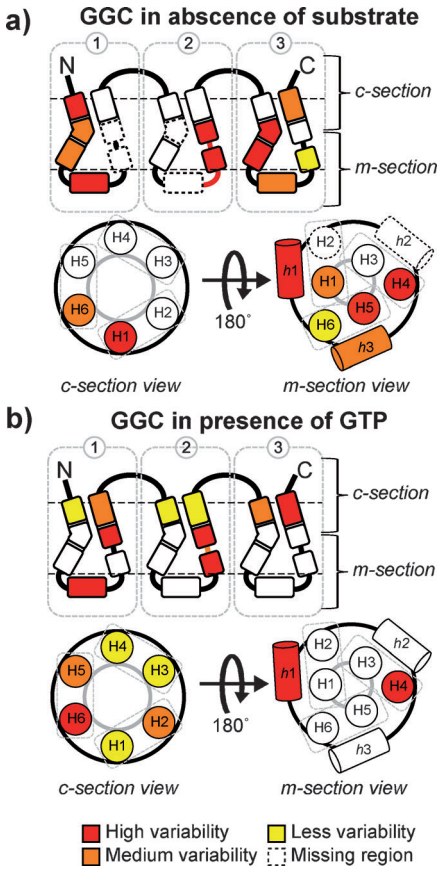

Figure 5. Mapping local GDO variation for GGC in the absence (a) and presence (b) of GTP. Local GDO variation is defined as the GDO difference between seven-residue segments that are shifted relative to each other by three residues.

heterogeneity, for example, GDO values vary significantly even within the H1, H4, and H5 helices (Figures 3a, 4a, and 5a). It has been proposed that TM helices of membrane proteins are often malleable, possibly because of the shifting of backbone hydrogen-bond partners during functional cycles of the proteins.[21] Although the implication of the structural plasticity of TM helices remains to be investigated, we propose that it is important in facilitating the large-scale conformational switch. GTP binding reduces local GDO variation in the P-kink motifs of domains I and III, which indicates partial stabilization of the central substrate-binding region in the middle of the transporter. This result is consistent with GTP binding to the pivot region of GGC as confirmed by the residue-specific K_D mapping in Figure 2c. GTP binding induces an asymmetry between the *c-section* and the *m-section* of the transporter.

In both apo and GTP-bound states of GGC, the local conformational heterogeneity is asymmetrically distributed with the largest dispersion observed for domain I of the protein. Moreover, GTP binding appears to significantly alter this distribution. This observation is coherent with previous MD simulation of AAC without inhibitor, and showed asymmetric behavior of the three domains.[22] The finding implies that structural rearrangements which interconvert *c*- and *m*-states may not be symmetric as suggested by the threefold pseudosymmetry of the carrier architecture. Conformational heterogeneity is the consequence of conformational plasticity, and we believe such plasticity is important for substrate assess to the apo state and for substrate release from the GTP-bound state.

Received: August 21, 2014
Revised: November 9, 2014
Published online: January 21, 2015

Keywords: conformation analysis · DNA · membranes · NMR spectroscopy · nucleotides

[1] O. Jardetzky, *Nature* **1966**, *211*, 969–970.
[2] a) M. Klingenberg, *Biochim. Biophys. Acta Biomembr.* **2008**, *1778*, 1978–2021; b) I. C. West, *Biochim. Biophys. Acta Rev. Biomembr.* **1997**, *1331*, 213–234.
[3] L. R. Forrest, R. Kramer, C. Ziegler, *Biochim. Biophys. Acta Bioenerg.* **2011**, *1807*, 167–188.
[4] a) G. B. Erkens, I. Hanelt, J. M. Goudsmits, D. J. Slotboom, A. M. van Oijen, *Nature* **2013**, *502*, 119–123; b) E. A. Morrison, G. T. DeKoster, S. Dutta, R. Vafabakhsh, M. W. Clarkson, A. Bahl, D. Kern, T. Ha, K. A. Henzler-Wildman, *Nature* **2012**, *481*, 45–50; c) L. R. Forrest, Y. W. Zhang, M. T. Jacobs, J. Gesmonde, L. Xie, B. H. Honig, G. Rudnick, *Proc. Natl. Acad. Sci. USA* **2008**, *105*, 10338–10343; d) Y. Zhao, D. Terry, L. Shi, H. Weinstein, S. C. Blanchard, J. A. Javitch, *Nature* **2010**, *465*, 188–193.
[5] F. Palmieri, G. Agrimi, E. Blanco, A. Castegna, M. A. Di Noia, V. Iacobazzi, F. M. Lasorsa, C. M. Marobbio, L. Palmieri, P. Scarcia, S. Todisco, A. Vozza, J. Walker, *Biochim. Biophys. Acta Bioenerg.* **2006**, *1757*, 1249–1262.
[6] E. R. Kunji, A. J. Robinson, *Curr. Opin. Struct. Biol.* **2010**, *20*, 440–447.
[7] a) E. Pebay-Peyroula, C. Dahout-Gonzalez, R. Kahn, V. Trezeguet, G. J. Lauquin, G. Brandolin, *Nature* **2003**, *426*, 39–44; b) J. J. Ruprecht, A. M. Hellawell, M. Harding, P. G. Crichton, A. J. McCoy, E. R. Kunji, *Proc. Natl. Acad. Sci. USA* **2014**, *111*, E426–434.
[8] M. J. Berardi, W. M. Shih, S. C. Harrison, J. J. Chou, *Nature* **2011**, *476*, 109–113.
[9] F. Palmieri, C. L. Pierri, *FEBS Lett.* **2010**, *584*, 1931–1939.
[10] a) S. Imai, M. Osawa, K. Takeuchi, I. Shimada, *Proc. Natl. Acad. Sci. USA* **2010**, *107*, 6216–6221; b) S. Imai, M. Osawa, K. Mita, S. Toyonaga, A. Machiyama, T. Ueda, K. Takeuchi, S. Oiki, I. Shimada, *J. Biol. Chem.* **2012**, *287*, 39634–39641; c) J. H. Chill, J. M. Louis, J. L. Baber, A. Bax, *J. Biomol. NMR* **2006**, *36*, 123–136.
[11] a) A. Gautier, J. P. Kirkpatrick, D. Nietlispach, *Angew. Chem. Int. Ed.* **2008**, *47*, 7297–7300; *Angew. Chem.* **2008**, *120*, 7407–7410; b) S. Reckel, D. Gottstein, J. Stehle, F. Lohr, M. K. Verhoefen, M. Takeda, R. Silvers, M. Kainosho, C. Glaubitz, J. Wachtveitl, F. Bernhard, H. Schwalbe, P. Guntert, V. Dotsch, *Angew. Chem. Int. Ed.* **2011**, *50*, 11942–11946; *Angew. Chem.* **2011**, *123*, 12148–12152; c) J. Stehle, R. Silvers, K. Werner, D. Chatterjee, S. Gande, F. Scholz, A. Dutta, J. Wachtveitl, J. Klein-Seetharaman, H. Schwalbe, *Angew. Chem. Int. Ed.* **2014**, *53*, 2078–2084; *Angew. Chem.* **2014**, *126*, 2110–2116.
[12] a) Y. Kofuku, T. Ueda, J. Okude, Y. Shiraishi, K. Kondo, M. Maeda, H. Tsujishita, I. Shimada, *Nat. Commun.* **2012**, *3*, 1045; b) R. Nygaard, Y. Zou, R. O. Dror, T. J. Mildorf, D. H. Arlow, A. Manglik, A. C. Pan, C. W. Liu, J. J. Fung, M. P. Bokoch, F. S. Thian, T. S. Kobilka, D. E. Shaw, L. Mueller, R. S. Prosser, B. K. Kobilka, *Cell* **2013**, *152*, 532–542; c) Y. Kofuku, T. Ueda, J. Okude, Y. Shiraishi, K. Kondo, T. Mizumura, S. Suzuki, I.

Shimada, *Angew. Chem. Int. Ed.* **2014**, *53*, 13376 – 13379; *Angew. Chem.* **2014**, *126*, 13594 – 13597.
[13] A. Vozza, E. Blanco, L. Palmieri, F. Palmieri, *J. Biol. Chem.* **2004**, *279*, 20850 – 20857.
[14] F. Delaglio, G. Kontaxis, A. Bax, *J. Am. Chem. Soc.* **2000**, *122*, 2142 – 2143.
[15] Y. Shen, F. Delaglio, G. Cornilescu, A. Bax, *J. Biomol. NMR* **2009**, *44*, 213 – 223.
[16] A. J. Robinson, E. R. Kunji, *Proc. Natl. Acad. Sci. USA* **2006**, *103*, 2617 – 2622.
[17] F. Palmieri, C. L. Pierri, A. De Grassi, A. Nunes-Nesi, A. R. Fernie, *Plant J.* **2011**, *66*, 161 – 181.
[18] J. R. Tolman, H. M. Al-Hashimi, L. E. Kay, J. H. Prestegard, *J. Am. Chem. Soc.* **2001**, *123*, 1416 – 1424.
[19] a) Y. Wang, E. Tajkhorshid, *Proc. Natl. Acad. Sci. USA* **2008**, *105*, 9598 – 9603; b) F. Dehez, E. Pebay-Peyroula, C. Chipot, *J. Am. Chem. Soc.* **2008**, *130*, 12725 – 12733.
[20] D. Di Marino, F. Oteri, B. Morozzo Della Rocca, I. D′Annessa, M. Falconi, *J. Mol. Model.* **2012**, *18*, 2377 – 2386.
[21] Z. Cao, J. U. Bowie, *Proc. Natl. Acad. Sci. USA* **2012**, *109*, 8121 – 8126.
[22] J. M. Johnston, S. Khalid, M. S. Sansom, *Mol. Membr. Biol.* **2008**, *25*, 506 – 517.

